GESEP – Gerência de Especialistas em Sistemas Elétricos de Potência

Título:

Novel adaptive saturation scheme for photovoltaic inverters with ancillary service capability.

Autores:

L. S. Xavier, V. M. R. de Jesus, A. F. Cupertino, V. F. Mendes and H. A. Pereira.

Publicado em:

8th International Symposium on Power Electronics for Distributed Generation Systems (PEDG)

Data da publicação:

2017

Citação para a versão publicada:

L. S. Xavier, V. M. R. de Jesus, A. F. Cupertino, V. F. Mendes and H. A. Pereira, "Novel adaptive saturation scheme for photovoltaic inverters with ancillary service capability," 2017 IEEE 8th International Symposium on Power Electronics for Distributed Generation Systems (PEDG), Florianopolis, 2017, pp. 1-8.

Novel Adaptive Saturation Scheme for Photovoltaic Inverters with Ancillary Service Capability

Lucas S. Xavier[1], Victor Magno R. de Jesus[1], Allan F. Cupertino[2], Victor F. Mendes[1], Heverton A. Pereira[3]

[1] Graduate Program in Electrical Engineering - Federal University of Minas Gerais - Av. Antônio Carlos 6627, 31270-901, Belo Horizonte, MG, Brazil

[2]Department of Materials Engineering, Federal Center for Technological Education of Minas Gerais - Av. Amazonas 5253, 30421-169, Belo Horizonte - MG, Brazil

[3]Electric Engineering Department, Federal University of Viçosa, 36570900, Viçosa, Brazil

e-mail: lsantx@gmail.com, allan.cupertino@yahoo.com.br, victormendes@cpdee.ufmg.br, heverton.pereira@ufv.br

***Abstract*—The insertion of grid connected photovoltaic (PV) in the power systems have occurred mainly at low and medium voltage. Besides, due to solar irradiance variation, these converters have excess capacity that can be used to provide ancillary services to the main grid. Therefore, this work is focused on the analysis of how PV inverters can perform ancillary services, supporting the grid. Control strategies for reactive power injection and harmonic current compensation are explored. Furthermore, the inverter current saturation for PV inverters is described. The current saturation plays an important role, once high currents can damage the inverter or reduce its lifetime. It is presented a novel adaptive saturation scheme for photovoltaic inverters with ancillary service capability. A Case study for single-phase PV inverters is presented, considering low and high irradiance level scenarios. The simulation results shown the effectiveness of the adaptive current saturation scheme, depicted in this work, for PV inverters.**

I. Introduction

Considering a scenario with high penetration of photovoltaic (PV) systems, grid-connected inverters with ancillary services capability have been an interesting research topic. In view of this fact, many works have proposed methodologies to compensate reactive power and current harmonics by means of photovoltaic inverters [1], [2].

The harmonic compensation of the nonlinear loads connected to the point of common coupling (PCC) has many tasks associated, as the harmonic detection methodology and the current control strategy [1], [3], [4]. However, the most important fact is the inverter current limitation, which can not be exceeded when the converter is providing ancillary services. The determination of a current limit is relatively simple for reactive power compensation. However, when harmonic components are compensated, it is very difficult to determine if there is inverter current margin to perform this ancillary service, once it is complex to calculate the inverter current peak by an analytical expression [3], [4].

In view of this fact, references [3], [4] propose the use of an anti-windup proportional-integral (PI) controller, which calculates the perceptual of harmonic compensation. However, the parameter adjustment of this controller is complex. Additionally, this strategy results in a poor dynamic behavior. In this context, this work proposed a new algorithm to provide dynamic saturation of the current reference of a photovoltaic inverter with ancillary services capability. Using this approach, the inverter can compensate partially the harmonic content of the load without exceed its rated current. Furthermore, the algorithm presents a fast response, resulting in a time response smaller than 3 cycles of fundamental frequency.

978-1-5090-5339-1/17/$31.00 2017 IEEE.

II. Single-Phase Grid-Connected PV System With Ancillary Service Capability

The single-phase grid-connected PV system with ancillary service capability is shown in Fig. 1. It is worth noting that electrical quantities represented by lowercase letters mean ac signals. On the other hand, electrical quantities represented by uppercase letter mean dc signals.

Reactive power support and current harmonic compensation require the measurement of the grid current. This is a relatively simple modification in the inverter scheme, which can increase considerably the inverter performance.

The electrical model of the PV panel, used in this work, is based on the mathematical model addressed in [5].

The dc/dc stage is commonly used to connect the solar array to the PV inverter [6], [7]. With dc/dc stage, it is possible to achieve an dedicated stage for maximum power point tracking (MPPT). Another advantage of dc/dc stage, specifically the boost converter, is to provide a voltage gain important to ensure that the DC-link has enough voltage level to keep the grid-connected PV inverter.

Generally, PV inverters are connected to the PCC through passive filters to suppress the harmonic components produced during the switching process. L filters are an attractive solution due to their simple implementation. However, in practice, the connection through LCL filters present a small cost-benefit ratio, once LCL filters present smaller volume, considering similar attenuation capacity. However, LCL filters can insert resonances in the power system. Two solutions to damp resonances are through passive elements, i.e., adding a resistor

in series with the filter capacitor, or through active damping techniques [8], [9], [10].

To perform the harmonic current compensation, the load current is estimated through the grid current and inverter current. This ensures that current measurements of all loads connected to the installation are obtained.

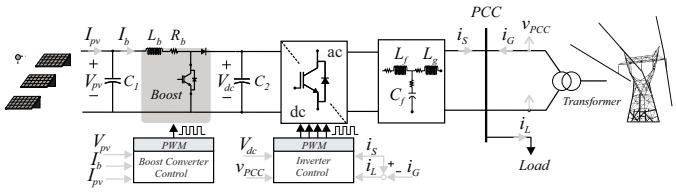

Fig. 1: Single-phase grid-connected photovoltaic system with ancillary service capability.

III. DC/DC STAGE CONTROL STRATEGY

The boost converter control loop is shown in Fig. 2 and it is used two PI controllers. This control loop consists of an outer loop responsible for controlling the solar array output voltage (V_{pv}) and an inner loop tuned to regulate the boost converter inductor current (I_b). Some works use only the voltage control in the dc/dc stage [6], [11]. On the other hand, the system may be more robust to disturbances if there are an outer loop and an inner loop control [7]. The voltage reference to the outer loop is calculated by a maximum power point tracking (MPPT) algorithm. In this work, the incremental conductance algorithm is used [12].

A small signal analysis is applied to obtain the transfer functions of the outer and inner boost control loop [7]. Considering the dc-link voltage constant (V_{dc}), these transfer functions are given by:

$$G_{id}(s) = \frac{I_b(s)}{d(s)} = \frac{V_{dc}}{L_b s + R_b}, \tag{1}$$

$$G_{vi}(s) = \frac{V_{pv}(s)}{I_b(s)} = -\frac{R_{eq}}{R_{eq} C_1 s + 1}, \tag{2}$$

where d is the duty cycle. The PV array should be linearized around the nominal operation point to obtain the boost converter model. Therefore, the solar array can be represented by a linear circuit composed by a voltage source and an equivalent series resistance (R_{eq}) [7].

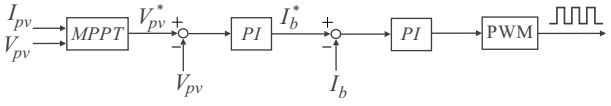

Fig. 2: Boost converter control loop.

IV. SINGLE-PHASE PV INVERTER CONTROL STRATEGY WITH ANCILLARY SERVICE CAPABILITY

Similarly to the dc/dc stage control strategy, the inverter control loop has an outer and an inner loop, as shown in Fig. 3. The outer loop is based on the voltage-squared control method.

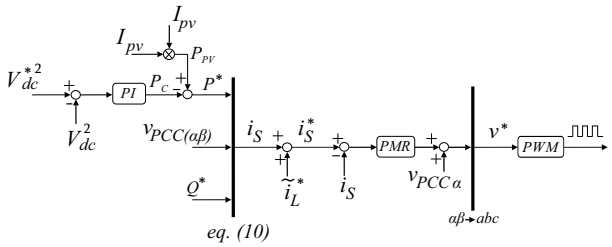

Fig. 3: Inverter control strategy with ancillary service capability.

A. Outer-Loop Control: dc-Link Voltage Control

The outer loop is based on the dc-link voltage control. The capacitor dynamic model of the dc-link can be obtained from the consideration of the energy stored W in this component, i.e.,

$$W = \frac{1}{2} C_2 V_{pv}^2. \tag{3}$$

The active power (P_C) must be equal to the time derivative of the energy stored on the capacitor, as given by:

$$P_c(t) = \frac{dW}{dt} = \frac{1}{2} C_2 \frac{dy(t)}{dt}, \tag{4}$$

where $y(t) = V_{pv}^2$.

Thus, (3) can be replaced in (4) and expressed in frequency domain by:

$$P_c(s) = P_{pv}(s) - P^*(s) = \frac{1}{2} C s Y(s). \tag{5}$$

A linear relation between the generated PV power (P_{pv}), the power injected by the inverter (P^*) and squared dc-bus voltage is obtained as being:

$$Y(s) = 2\frac{P_{pv}(s) - P^*(s)}{C_2 s}. \tag{6}$$

Considering P_{pv} as a disturbance and a PI controller given by:

$$G_{CV}(s) = K_{p,dc} + \frac{K_{i,dc}}{s}. \tag{7}$$

Therefore, the closed-loop transfer function is given by:

$$\frac{Y(s)}{Y^*(s)} = \frac{K_{p,dc} s + K_{i,dc}}{\frac{1}{2} C_2 s^2 + K_{p,dc} s + K_{i,dc}}. \tag{8}$$

The closed-loop block diagram is shown in Fig. 4.

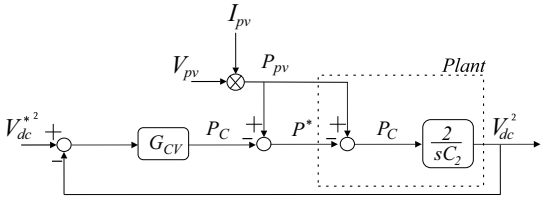

Fig. 4: Closed-loop block diagram for DC-link voltage control.

B. Inner-Loop Control: Current Inverter Control

The inner-loop is responsible to the inverter current control. In Fig. 1, disregarding the capacitor dynamic of the LCL filter for lower frequency signals, the system model is given by:

$$v_S - Ri_S - L\frac{di_S}{dt} - v_{PCC} = 0, \tag{9}$$

where L and R are the inductance equivalent and resistance equivalent of the LCL filter, respectively. V_{PCC} and V_S are the PCC voltage and the inverter voltage output, respectively. The inverter current reference (i_S) is obtained by the following equation coming from instantaneous power theory [2], [13]:

$$\begin{bmatrix} i_{S\alpha} \\ i_{S\beta} \end{bmatrix} = \frac{2}{v_{PCC\alpha}^2 + v_{PCC\beta}^2} \begin{bmatrix} v_{PCC\alpha} & v_{PCC\beta} \\ v_{PCC\beta} & -v_{PCC\alpha} \end{bmatrix} \begin{bmatrix} P^* \\ Q^* \end{bmatrix}, \tag{10}$$

where P^* is the active power reference to be injected in the grid by the PV system. Q^* is the reference for reactive power compensation. $i_{S\alpha\beta}$ is the inverter current in stationary reference frame. The voltage components $v_{PCC\alpha\beta}$ are PCC voltages in $\alpha\beta$ stationary reference frame. In single phase-system, these two components can be emulated by a second order generalized integrator (SOGI) [14]. It is important to note that only α-component is controlled in single-phase system.

The current harmonic ($\tilde{i}_L^*$) is added to the inverter current in order to achievement the harmonic compensation.

The inverter current control is made by means of proportional multi-resonant controllers (PMR) adjusted in each harmonic frequency to be compensated. The PMR transfer function can be represented by [15]:

$$G_C(s) = K_P^r + \sum_{h=1}^{n} K_{i,h}^r \overbrace{\frac{s}{s^2 + \omega_h^2}}^{R_h(s)}, \tag{11}$$

where K_p^r is the proportional gain, h is the harmonic order ($h = 1, 2, 3..., n$), ω_h are resonant frequencies, $K_{i,h}^r$ are the resonant gains for each harmonic frequency.

The PMR controller has high gains at its resonant frequencies. Thereby, the terms $R_h(s)$ are responsible for tracking the current components at ω_h frequencies. K_p^r and $K_{i,h}^r$ are adjusted in accordance with reference [15], which considers the crossover frequency of the controller and its relationship with the critical point on Nyquist diagram.

The discretization method used in $R_h(s)$ is the Tustin with prewarping. This technique avoids the shift of the resonant frequency for which it was tuned, in this way the $R_h(z)$ is given by [16]:

$$R_h(z) = \frac{sin(\omega_h T_S)}{2\omega_h} \frac{1 - z^-2}{1 - 2z^{-1}cos(\omega_h T_S) + z^-2}, \tag{12}$$

where T_S is the sampling period.

V. Load Reactive Power and Harmonic Current Detection

In this work, the information of the load reactive power and harmonic current are extracted using the conservative power theory (CPT). Using this theory, it is possible to separate a current signal in three orthogonal components: the active component, the harmonic component and the reactive component. The description detailed about the CPT is shown in [17].

According to the CPT, under periodic general condition, the average active power is given by:

$$P = \frac{1}{T}\int_t^{t+T} v_{PCC} i_L dt, \tag{13}$$

where (v_{PCC}) and (i_L) are the instantaneous values of the voltage and current in the load. T is the inverse of the fundamental frequency. According to CPT, the active current (i_{La}) can be defined as the necessary current to carry active power and it is represented by [17]:

$$i_{La} = \frac{P}{V^2} v_{PCC}, \tag{14}$$

where V is the RMS voltage of v_{PCC}.

Similarly to the average active power calculation, the average reactive energy (W) can be calculated as:

$$W = \frac{1}{T}\int_t^{t+T} \hat{v}_{PCC} i_L dt, \tag{15}$$

where $\hat{v}_{PCC}$ is the unbiased time integral of v_{PCC}, given by:

$$\hat{v}_{PCC}(t) = \int_0^t v_{PCC} dt - \frac{1}{T}\int_0^{t+T}\int_0^t v_{PCC} d\tau dt. \tag{16}$$

The reactive power is calculated from the average reactive energy and the fundamental frequency ω. It is given by:

$$Q = \omega W. \tag{17}$$

The reactive current i_{Lr} is defined as the necessary current to carry reactive power. It is given by:

$$i_{Lr}(t) = \frac{W}{\hat{V}^2} \hat{v}_{PCC}. \tag{18}$$

The third current component does not transmit active and reactive power. In this current component, there are harmonic components due to the nonlinear load. Thus, it is calculated by:

$$\tilde{i}_L = i_L - i_{La} - i_{Lr}. \tag{19}$$

VI. Adaptive Saturation Scheme for PV Inverters

Important issues arise when new capabilities are integrated in PV inverters. In order to avoid inverter damages and to preserve its lifetime, the inverter maximum current may not be exceeded. Thereby, strategies for PV inverter current limitation are required during ancillary services support. The critical point it is when harmonic current compensation is

involved. When there are multiple frequencies in the current signal, analytical expressions for inverter current limitation are complex. Therefore, reference [4] have proposed an algorithm making possible to the inverter to perform harmonic current compensation without exceeding its maximum current. This algorithm will be addressed in this section and a new algorithm is proposed further.

A. Reactive Power Saturation Scheme

The load reactive power detected by the conservative power theory (Q) can be limited by a simple saturator, this depends of the active power (P^*) being injected by the PV inverter [4]. Therefore, the saturation threshold of the reactive power to be compensated (Q^*) can be found by phasor calculation, being:

$$-\sqrt{S_m^2 - P^{*2}} \leq Q^* \leq +\sqrt{S_m^2 - P^{*2}}, \tag{20}$$

where S_m^* is the inverter maximum apparent power.

B. Harmonic Current Saturation Based on Anti-Windup PI Controllers (HCS-AWPI)

In literature, it is addressed a harmonic current saturation scheme for single-phase PV inverter based on closed-loop control with an anti-windup PI controller saturated from 0 to 1 [4], called here of HCS-AWPI strategy. The PI controller action ponders the harmonic compensation, ensuring the inverter current reference does not exceeded its maximum value. This closed-loop control is illustrated in Fig. 5.

The current i_S calculated by the outer loop and added to the load harmonic current ($\tilde{i}_L^*$), resulting in the inverter current reference i_S^*. Samples of this current are stored in a vector and its maximum (I_m) is extracted each cycle. Next step, I_m is compared to the inverter maximum current (I_m^*). The anti-windup PI controller, limited between 0 and 1, calculates the compensation factor (K_h) to determine if the compensation will be total, partial or null. However, like any control loop, this system can be lead to instabilities due to external disturbances. Besides, it is complex to tune this PI controller, once the plant model is unknown.

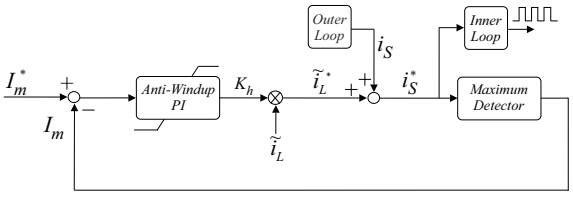

Fig. 5: Harmonic current saturation strategy for PV inverters based on anti-windup PI controller.

C. Harmonic Saturation Algorithm (HSA)

This work proposes a harmonic saturation algorithm (HSA). This strategy does not require a PI controller to perform the partial harmonic compensation. The compensation factor (K_h) is calculated by an simple algorithm that analyses, each current fundamental cycle, the contribution of the harmonic current

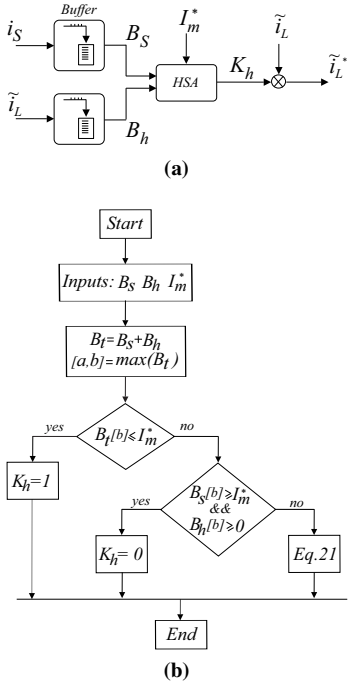

Fig. 6: Harmonic current saturation scheme:(a) Block diagram. (b) Flowchart of the harmonic saturation algorithm (HSA).

to the maximum value of the inverter reference current. This harmonic saturation scheme is presented in Fig. 6(a).

The harmonic content of the load current ($\tilde{i}_L$) and the inverter current reference (i_S) with only fundamental frequency are stored in two buffers with size of a fundamental frequency cycle. these buffers are processed by the HSA. The flowchart of this algorithm is shown Fig. 6(b). The step-by-step of this algorithm is

- The buffers of i_S and $\tilde{i}_L$ are declared as being B_s and B_h, respectively;
- The buffer B_t which represents the total inverter current reference (i_S^*), including fundamental and harmonic frequencies, is obtained by summing B_s and B_h. After, B_t maximum value is extracted, being a the value and b the position of this maximum value at the buffer. Thus, $B_s[b]$ and $B_h[b]$ represent the contribution of B_s and B_h to the B_t maximum value, respectively. It is worth highlighted that $B_s[b]$ is always less than or equal to I_m^*, it is already ensured by the reactive power saturation.
- If the B_t maximum value (B_t[b]) is less than or equal to inverter maximum current (I_m^*), there is current margin to compensate all load current harmonic content (K_h = 1).
- Otherwise, if $B_s[b]$ is greater than or equal to I_m^* and $B_h[b]$ is greater than or equal to zero, there is no current margin for harmonic compensation (K_h = 0). This fact occurs because $B_s[b]$ already reached the inverter current limitation.
- If $B_s[b]$ is equal to I_m^* or the $B_h[b]$ is less than or equal to zero, there is current margin for partial harmonic

compensation. Thus, K_h needs to ponder the load harmonic current, ensuring that the $B_h[b]$ does not exceed the inverter current limit. In this case, K_h can be calculated as:

$$K_h = \frac{I_m^* - B_s[b]}{B_h[b]}. \quad (21)$$

Fig. 7 illustrates the HSA operation during load current harmonic compensation. In this case, the inverter maximum current (I_m^*) is 19.3 A. The Fig. 7(a) shows the current harmonic compensation without HSA action. The contribution of the inverter current reference with only fundamental frequency component (i_S) to the maximum value of $i_S^* = i_S + \tilde{i}_L$ is 14.5 A. On the other hand, the contribution of the load harmonic current ($\tilde{i}_L$) to the maximum value of i_S^* is 12 A. Therefore, the i_S^* maximum value is 26.5 A and it exceeds the inverter current limitation. Keeping i_S fixed, the only way to reduce i_S^* peak is reducing $\tilde{i}_L$ contribution. Thereby, the HSA calculates, through eq. (21), how much $\tilde{i}_L$ can contribute to the i_S^* peak. The Fig 7(b) illustrated that the i_h is pondered by the K_h in 40 $\%$, resulting in i_h^* and its contribution becomes 4.8 A. Thus, the maximum value of $i_S^* = i_S + \tilde{i}_L^*$ is 19.3 A, respecting the inverter maximum current.

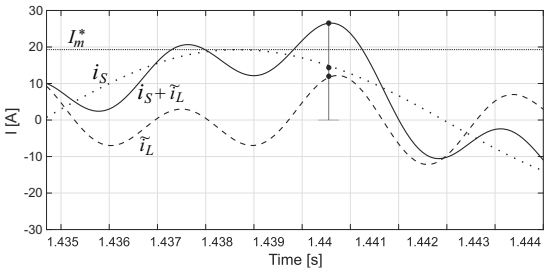

(a)

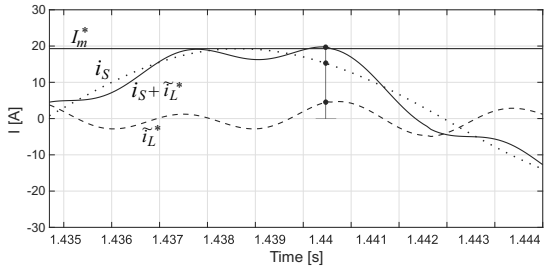

(b)

Fig. 7: Waveforms details of the current during harmonic current compensation(a) Without HSA action. (b) With HSA action. Currents: inverter maximum current (I_m^*); inverter current reference with only fundamental frequency component (i_S); load harmonic current ($\tilde{i}_L$); load saturated harmonic current ($\tilde{i}_L^*$).

It can be concluded with these analyses that the K_h will only be zero if the contribution of i_S to the i_S^* maximum value to coincide with its own maximum. In other words, the strategies presented in this work do not guarantee priority of ancillary services. It is possible to compensate harmonic currents even without inverter margin current for reactive power compensation, and vice-versa.

VII. Results

A case study is performed to validate the adaptive saturation scheme for PV inverters with ancillary services capability, in order to ensure that these devices works below their maximum current. Reactive power compensation and harmonic current compensation are the ancillary services performed in this work. It is used a solar array with 2 parallel strings with 6 modules of 250 W in series. The inverter dc-link voltage is controlled in 390 V. The simulation was implemented in PLECS and Matlab environments. Parameters of simulation system are presented in TABLE I.

The reactive power compensation and harmonic current compensation are enabled in 0.4 and 0.6 seconds, respectively. Initially, the simulated solar irradiance level is 300 W/m^2 until 1.2 seconds. Afters this time, the solar irradiance increases to 650 W/m^2. From 1.8 seconds, the solar irradiance is 1000 W/m^2.

TABLE I: Case study parameters.

System Parameters	**Value**
Switching frequency	12 kHz
Sampling frequency	12 kHz
PCC parameters	220 V/60 Hz
Boost Converter Parameters	**Value**
L_b / R_b	0.8 mH / 10 $m\Omega$
C_1	500 μF
Inverter Parameters	**Value**
Maximum Power	3.4 kVA
Maximum Peak Current	22.17 A
LCL Filter Parameters	**Value**
L_f = L_g	1 mH / 18 $m\Omega$
r_d	4 Ω
C_f	3.8 μF
Boost Converter Control	**Value**
Outer Loop PI Gains	$K_p = 0.7540$ and $K_i = 132.2776$
Inner Loop PI Gains	$K_p = 0.0155$ and $K_i = 0.1933$
Inverter Control	**Value**
Outer Loop PI Gains	$K_{p,dc} = 0.2073$ and $K_i = 2.3687$
Inner Loop PI Gains	$K_p^r = 14.83$ and $K_i^r = 2000$
HCS-AWPI Control	**Value**
K_p	0.08
K_i	5

A resistive-inductive load of 4 kVA, with power factor of 0.91, is connected to the PCC. It is used a diode rectifier model to simulate a nonlinear load.

When the solar irradiance is 300 W/m^2 in $0.6 < t < 1$ seconds, the inverter supplies partially the load active power, as can be seen in Fig. 8. At this same time interval, the PV inverter has current margin to supply all load reactive power. When the harmonic current compensation is enabled in 0.6 seconds, there is also inverter current margin to compensate all load harmonic current and thus the compensation factor (K_h) is 1, as shown in Fig. 9. In this figure, it is illustrated the factor K_h calculated by both algorithms presented in this work (HSA and HCS-AWPI). The PI gains of the HCS-AWPI strategy are tuned in order to achieve the best relationship between fast response and oscillations. System current waveform details during harmonic current compensation using harmonic saturation algorithm (HSA) are shown in Fig.10. Note that in $0.6 < t < 1$, the grid current waveform is improved, as illustrated in Fig. 10(b). The grid current total harmonic distortion decreases (THD) from 60.50% to 5.25%. In contrast,

the inverter current THD increases from 2.62% to 94.87% due to the harmonic current compensation, as shown in Fig. 10(c).

In $1 < t < 1.4$ seconds, the solar irradiance is 650 W/m^2. Thus, the inverter supplies partially the load active power, as can be seen in Fig. 8. There is no inverter current margin to compensate all the load harmonic current and thus the K_h is 0.57, as shown in Fig. 9. In other words, only 57 $\%$ of the harmonic current are compensated. Thereby, the grid current THD increase from 5.25% to 42.87%, as illustrated in Fig. 10(b). In contrast, the inverter current THD decrease from 94.87% to 38.89%. The space phasor path of the inverter current is illustrated in Fig. 10(d) in $1 < t < 1.4$. In this graph it is possible to note the importance of the harmonic saturation strategy. In steady-state, the inverter operates with current equals to its rated current. If any saturation strategy is employed, the obtained space phasor path is illustrated in Fig. 10(e). In this case, the peak current is larger than the rated current, fact which can reduce the converter lifetime.

In $1.4 < t < 1.8$ seconds, the solar irradiance is 1000 W/m^2. Thus, the inverter supplies partially the load active power, as can be seen in Fig. 8 and the harmonic current compensation is near zero. Nevertheless, the load reactive power is fully compensated. Thereby, the grid current THD increase from 42.87% to 255%, as illustrated in Fig. 10(b). This high THD level can be explained due to few fundamental component in the grid current and the high level of harmonic content. The inverter current THD decrease from 38.89% to 3.58%.

The load demand (active power + reactive power + harmonic content) is doubled after 1.8 seconds. In this case, the inverter supplies partially the load reactive power and the harmonic compensation still remains null ($K_h = 0$).

Fig. 11 shows the current waveform details of the system using HCS-AWPI strategy for this same case study. Comparing Fig. 10 with Fig. 11, it is possible to note that the grid current THD is a little higher using HCS-AWPI strategy than using HSA method. The major difference was 6 $\%$ in $1.4 < t < 1.8$. However, the most important differences are in the response time and the oscillations of the compensation factor K_h. The current dynamic of the HAS strategy has a faster response than HCS-AWPI method. The current dynamic reaches the steady state in less than 3 cycles using HSA strategy.

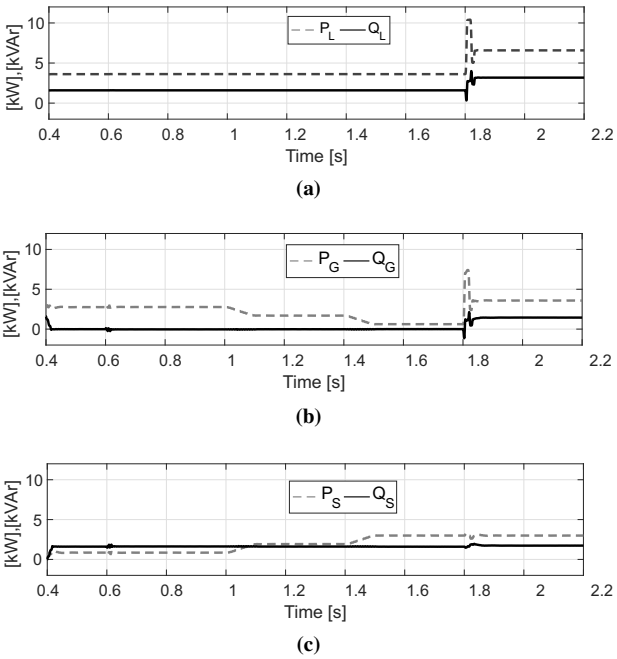

Fig. 8: Active power (P) and reactive power (Q) dynamic of the system with reactive power compensation capability.(a) Load power. (b) Grid power.(c) Inverter power.

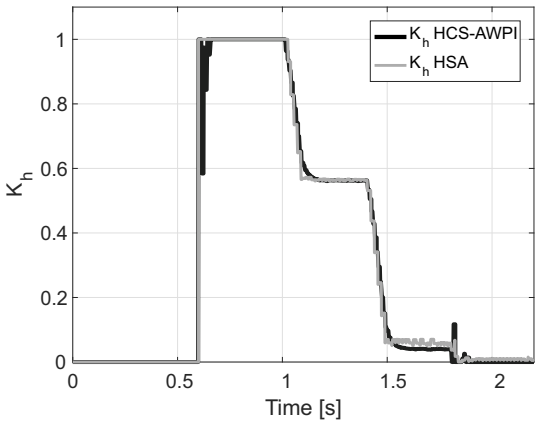

Fig. 9: Compensation factor K_h.

VIII. Conclusions

This work presented a grid-connected photovoltaic system based on inverter ancillary services capability. This concept consists in aggregate to the PV inverter control strategy other functions such as harmonics and reactive power compensation.

A novel adaptive saturation scheme for photovoltaic inverters with ancillary service capability was proposed in order to compensate partially reactive power and harmonic current of loads connected to the point of common coupling. The strategy to compensate partially the load harmonic current is based on a harmonic saturation algorithm, ensuring that the inverter works below its maximum current and thus preserving its lifetime. Simulations have shown that the grid current THD was reduced and the reactive power was compensated.

Furthermore, the harmonic saturation algorithm was compared with another strategy present in the literature for partially current harmonic compensation. However, the parameter adjustment this another strategy is complex and its dynamic behaviour is poor. Simulations have shown that the harmonic saturation algorithm proposed by this work presents faster response and it is more robust to the oscillations during transients.

Acknowledgment

This work has been supported by the Brazilian agency CAPES.

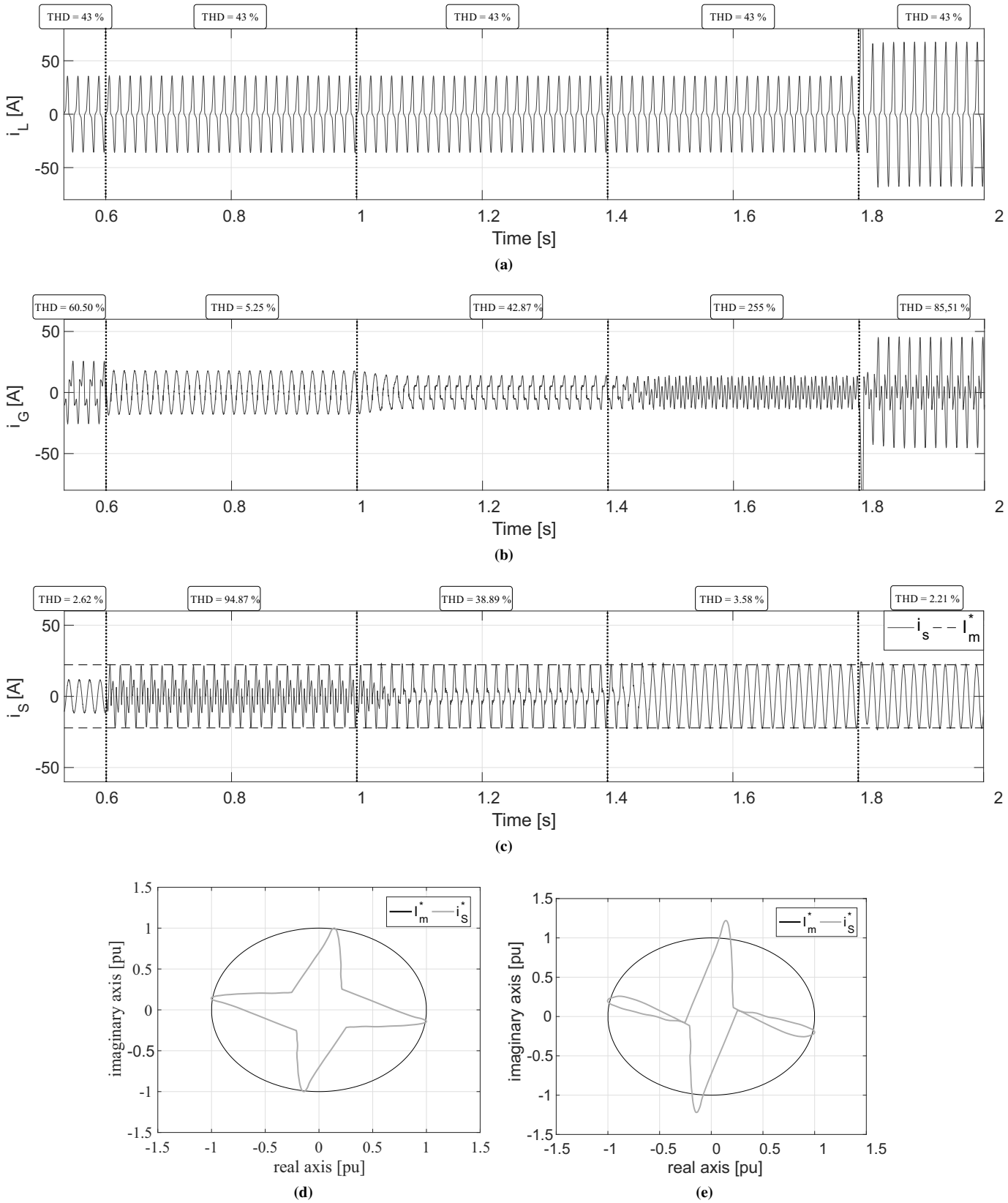

Fig. 10: System current waveform details during harmonic current compensation using harmonic saturation algorithm HSA.(a) Load current. (b) Grid current.(c) Inverter current.(d) Inverter current space phasor path considering the dynamic saturation strategy HAS in $1 < t < 1.4$ seconds.(e)Inverter Current space phasor path when no strategy for current limitation is employed in $1 < t < 1.4$.

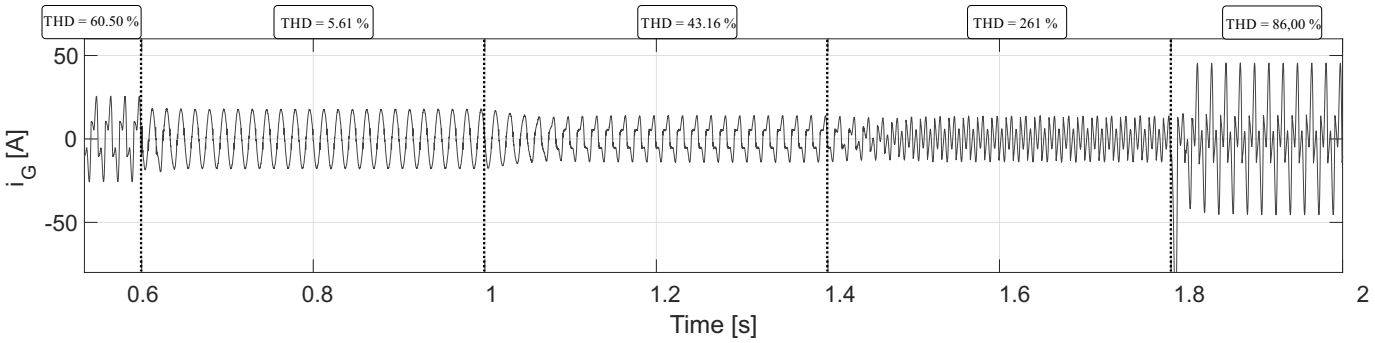

(a)

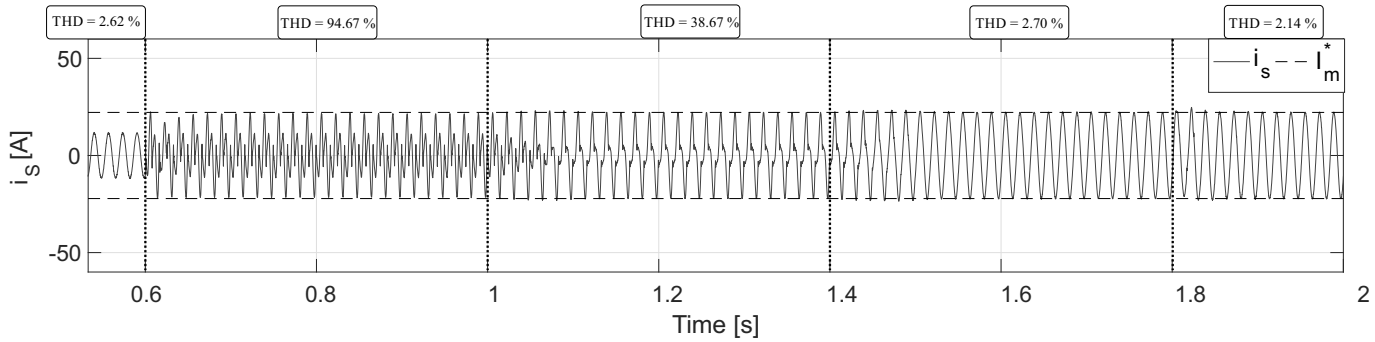

(b)

Fig. 11: System current waveform details during harmonic current compensation using HCS-AWPI strategy.(a) Load current. (b) Grid current.

The authors would like to thank the Brazilian agencies CAPES, FAPEMIG and CNPQ, which supported this work.

REFERENCES

[1] J. P. Bonaldo and J. Antenor Pomilio, "Multi-functional use of single-phase power converters," in *Innovative Smart Grid Technologies Latin America (ISGT LA), 2013 IEEE PES Conference On*, 2013, pp. 1–6.

[2] J. He, Y. W. Li, F. Blaabjerg, and X. Wang, "Active Harmonic Filtering Using Current-Controlled, Grid-Connected DG Units With Closed-Loop Power Control," *IEEE Transactions on Power Electronics*, vol. 29, no. 2, pp. 642–653, 2014.

[3] L. S. Xavier, A. F. Cupertino, and H. A. Pereira, "Adaptive saturation scheme for a multifunctional single-phase photovoltaic inverter," in *IEEE/IAS International Conference on Industry Applications*, 2014, pp. 1–8.

[4] H. A. Pereira, L. S. Xavier, A. F. Cupertino, and V. F. Mendes, "Single-phase multifunctional inverter with dynamic saturation scheme for partial compensation of reactive power and harmonics," *17th European Conference on Power Electronics and Applications*, pp. 1–10, 2015.

[5] M. G. Villalva, J. R. Gazoli, and E. R. Filho, "Comprehensive Approach to Modeling and Simulation of Photovoltaic Arrays," *IEEE Trans. Power Electron.*, vol. 24, no. 5, pp. 1198–1208, 2009.

[6] A. Sangwongwanich, Y. Yang, and F. Blaabjerg, "High-Performance Constant Power Generation in Grid-Connected PV Systems," vol. 31, no. 3, pp. 1822–1825, 2016.

[7] M. G. G. Villalva, T. G. G. de Siqueira, and E. Ruppert, "Voltage regulation of photovoltaic arrays: small-signal analysis and control design," *IET Power Electronics*, vol. 3, no. 6, p. 869, 2010.

[8] R. Peña-Alzola, M. Liserre, F. Blaabjerg, M. Ordonez, and Y. Yang, "LCL-Filter Design for Robust Active Damping in Grid-Connected Converters," *IEEE Trans. Ind. Informat.*, vol. 10, no. 4, pp. 2192–2203, 2014.

[9] M. Liserre, F. Blaabjerg, and S. Hansen, "Design and control of an LCL-filter-based three-phase active rectifier," *IEEE Transactions on Industry Applications*, vol. 41, no. 5, pp. 1281–1291, 2005.

[10] W. Wu, Y. He, T. Tang, and F. Blaabjerg, "A New Design Method for the Passive Damped LCL and LLCL Filter-Based Single-Phase Grid-Tied Inverter," *IEEE Trans. Ind. Electron.*, vol. 60, no. 10, pp. 4339–4350, 2013.

[11] F. Blaabjerg, R. Teodorescu, M. Liserre, and A. V. Timbus, "Overview of control and grid synchronization for distributed power generation systems," *IEEE Transactions on Industrial Electronics*, vol. 53, no. 5, pp. 1398–1409, 2006.

[12] D. Sera, L. Mathe, T. Kerekes, S. V. Spataru, and R. Teodorescu, "On the Perturb-and-Observe and Incremental Conductance MPPT Methods for PV Systems," *IEEE Journal of Photovoltaics*, vol. 3, no. 3, pp. 1070–1078, 2013.

[13] H. Akagi, Y. Kanazawa, and A. Nabae, "Instantaneous Reactive Power Compensators Comprising Switching Devices without Energy Storage Components," *IEEE Trans. Ind. Appl.*, vol. IA-20, no. 3, pp. 625–630, 1984.

[14] R. Teodorescu, M. Liserre, and P. Rodriguez, *Grid Converters for Photovoltaic and Wind Power Systems*. Wiley-IEEE Press, 2011.

[15] A. G. Yepes, F. D. Freijedo, O. Lopez, and J. Doval-Gandoy, "Analysis and Design of Resonant Current Controllers for Voltage-Source Converters by Means of Nyquist Diagrams and Sensitivity Function," *IEEE Transactions on Industrial Electronics*, vol. 58, no. 11, pp. 5231–5250, 2011.

[16] A. G. Yepes, F. D. Freijedo, J. Doval-Gandoy, Ó. López, J. Malvar, and P. Fernandez-Comesaña, "Effects of Discretization Methods on the Performance of Resonant Controllers," *IEEE Trans. Power Electron.*, vol. 25, no. 7, pp. 1692–1712, 2010.

[17] P. Tenti, H. K. M. Paredes, and P. Mattaveli, "Conservative Power Theory, a Framework to Approach Control and Accountability Issues in Smart Microgrids," *IEEE Trans. Power Electron.*, vol. 26, no. 3, pp. 664–673, 2011.